Unconventional mechanics of lipid membranes: a potential role for mechanotransduction of hair cells stereocilia

Jichul Kim PhD,
Department of Mechanical Engineering, Stanford University, Stanford, California

Correspondence
Jichul Kim, jichul0kim@kaist.ac.kr
(Current address: Department of Mechanical Engineering, Korea Advanced Institute of Science and Technology, 291 Daehak-ro, Yuseong-gu, Daejeon, Republic of Korea 305-338)

Keywords
Lipid bilayer, lipid flow, hair cell mechanotransduction, gating spring, tip link, nonlinearity

Abstract

A force conveying role of the lipid membrane is now an accepted hypothesis across various mechanoreceptors. However, such a mechanism is still not fully understood for mechanotransduction in the hair bundle of auditory sensory hair cells. A major goal of this theoretical assessment is to investigate the role of the lipid membrane in auditory mechanotransduction, especially in generating nonlinear bundle force vs. displacement measurements – one of the main features of auditory mechanotransduction. To this end, a hair bundle model that generates lipid membrane tented deformation in the stereocilia is developed. A computational analysis of the model not only reproduces nonlinear bundle force measurements but also generates membrane energy that is potentially sufficient to activate the mechanosensitive ion channel of the hair cell. In addition, the model provides biophysical insight into the following: the likelihood that the channel must be linked in some way to the tip link; how the interplay of the bending and stretching of the lipid bilayer may be responsible for the nonlinear force vs. displacement response; how measurements of 'negative stiffness' may be a function of the rotational stiffness of the rootlets; and how standing tension of the tip link is required to interpret migration of the nonlinear force vs. displacement and activation curves. The foregoing are all features of hair cell mechanotransduction, the biophysical mechanism of which has proved elusive for the last three decades.

INTRODUCTION

Auditory mechanosensation starts when the sensory hair cells of the inner ear, a part of the organ of Corti within the cochlea, are mechanically stimulated in response to sound, creating pressure waves between the cochlea compartments. Each hair cell features an apically located bundle of stereocilia of varying lengths extending from its top side, forming an elaborate structure with linkages connecting the tips of adjacent stereocilia with one another – features known as “tip links”. When these bundles of stereocilia, or “hair bundles”, are deflected in response to sound in the cochlea, they generate electrical signals that can trigger a sensation of hearing once they reach the brain (1). When a hair bundle is deflected, tension is produced in the stereociliary tip links, which in turn release energy used for the activation of the mechanosensitive (MS) transduction channel, which is presumed to be located within the tip complex of each stereocilium (2).

Consistent with studies on hair bundles of many different organ systems and animal species, the unconventional nonlinear force vs. displacement relationship dictates that the minimum stiffness is generated with the intermediate displacement of bundles (3-5). As this nonlinear force vs. displacement measurement is a central feature of hair bundle mechanics, and mechanotransduction activation, understanding the underlying molecular and biophysical components is crucial to overall understanding of auditory neuroscience.

Traditionally, the gating spring model suggests that hair bundle nonlinear force vs. displacement measurement results from gate opening of the hair cell MS channel (6). However, a long standing problem with this hypothesis is that the length estimates for the channel gating are quite large (more than 10nm) (3, 4). Here, an alternative theory is proposed to determine if deformation of the lipid membrane of the stereocilia induces this nonlinearity, and to elucidate the potential influence of the lipids in activation of the hair cell MS channel.

To this end, a biophysical hair bundle model based on viscoelastic lipid membrane system of the stereocilia is developed. This model considers elastic and hydrodynamic responses of the lipid membrane under ciliary cytoskeleton interaction. Although the model reproduces the nonlinear force measurement from turtle auditory papilla hair cell bundles in this work, the theory can be applied to hair bundles in any system of any species with some alterations in geometry. Furthermore, the model provides biophysical insights into many important aspects of the hair bundle mechanotransduction – such as channel activation and its relation with the bundle nonlinearity, negative stiffness, linearization, and migration components of the nonlinear bundle force measurement, for which the underlying mechanism has remained elusive during the past three decades.

METHODS

Description of biophysical hair bundle model

The model considers two basic components. The first is the rigid body kinematic component of the bundle that describes the motion of the side links, tip links, and rigid stereocilia and the translation of their motion to the membrane deformation in the stereocilia. When the bundle is displaced, stereocilia bend about their base from the resting position by deflecting roots (Fig. 1B). Here, the stiffness of the rootlet is parameterized with the rotational spring. The stereocilia are rigid and increasing in height toward a taller edge. Also, they are linked to each other by side- and tip links (Fig. 1A). The side links function to ensure that the hair bundle deflects coherently, and are able to slide along the stereocilia height (7-9). Both side

and tip links are considered to be inextensible (10).

The second component is the model for the lipid bilayer membrane of stereocilia. The lipid membrane of a coarse-grained continuum using theory originally introduced by Canham and Helfrich (11, 12) is presented as two regions in this model: a "tented-tip region" into which the tip link inserts and a "cytoskeleton-coupled region" where the membrane is more tightly associated with the cytoskeleton (Figs. 1C and D). In the tented-tip region, the membrane is stretchable to the tangential direction of the membrane and flexible (i.e. bendable) to change the curvature of the surface, while in the cytoskeleton-coupled region the membrane is not flexible although it is still stretchable. Therefore, the tip region can separate from the underlying cytoskeleton when mechanically perturbed whereas the cytoskeleton-coupled region maintains constant curvature of the cytoskeleton. In addition, the lipid mobility in the cytoskeleton-coupled region is parameterized with the diffusion constant but it is considered quasi-statically in the tented-tip region. Since the tented region is presumably not interacting with the cytoskeleton, lipid viscosity will be minimal here while it is significant in the cytoskeleton-coupled region (13). Therefore, lipid molecules quickly reorganize their distribution to have uniform lipid area density in the tented region, but a considerable lipid density gradient can be generated in the cytoskeleton-coupled region. The radius of the interface of the two regions is termed r_b and can be systematically varied.

The interaction of the membrane and cytoskeleton, central to this model, is not a heretical idea; the possibility has already been biologically characterized for the stereocilia. First, the morphology suggests that the upper tip link insertion is maintained rigid by a plaque containing a variety of important molecules such as harmonin and whirlin (1) while membrane tenting is often observed with electron microscopy on the lower insertion site (10, 14-16). Second, the electron microscopy study confirmed the membrane-cytoskeleton connection along the stereocilia and more recent experiments even identified proteins such as radixin and myosin IIIa as potential crosslinker molecules of this connection (17, 18). Thus, the assumption regarding the membrane-skeleton interaction in both the tented-tip region and the cytoskeleton-coupled region is supported well by existing morphological and functional data.

A flow diagram of model components and their interactions is presented in Fig. S1. Briefly, a prescribed stimulus of the bundle is introduced and translated kinematically to the tip link lower insertion point, which gives the magnitude of the membrane-tip displacement for each stereocilium. When the membrane is pulled, the tented-tip membrane undergoes elastic deformation associated with bending and stretching, while the viscoelastic property of the cytoskeleton-coupled region results in non-uniform stretching of that region, which ultimately modulates lipid flow to the tented region. Therefore, elastic deformations together with fluidic interactions between the two partitioned regions determine the tip link force and free energy density of the membrane. Finally, the bundle force is determined using the system equation (see Eqs. 1 and 2 in Method section), which expresses the overall moment equilibrium of the bundle. From this model, the tip link force, hair bundle force, and free energy density at specific points in the lipid membrane in response to a hair bundle deflection can be determined. A video that includes the bundle motion, deformed shape, and free energy density profile for the tented tip region and the lipid density profile for a single stereocilium in response to a hair bundle displacement of 50 *nm* is available in the Supporting Material (SM). Table 1 summarizes the primary parameter values used in the model.

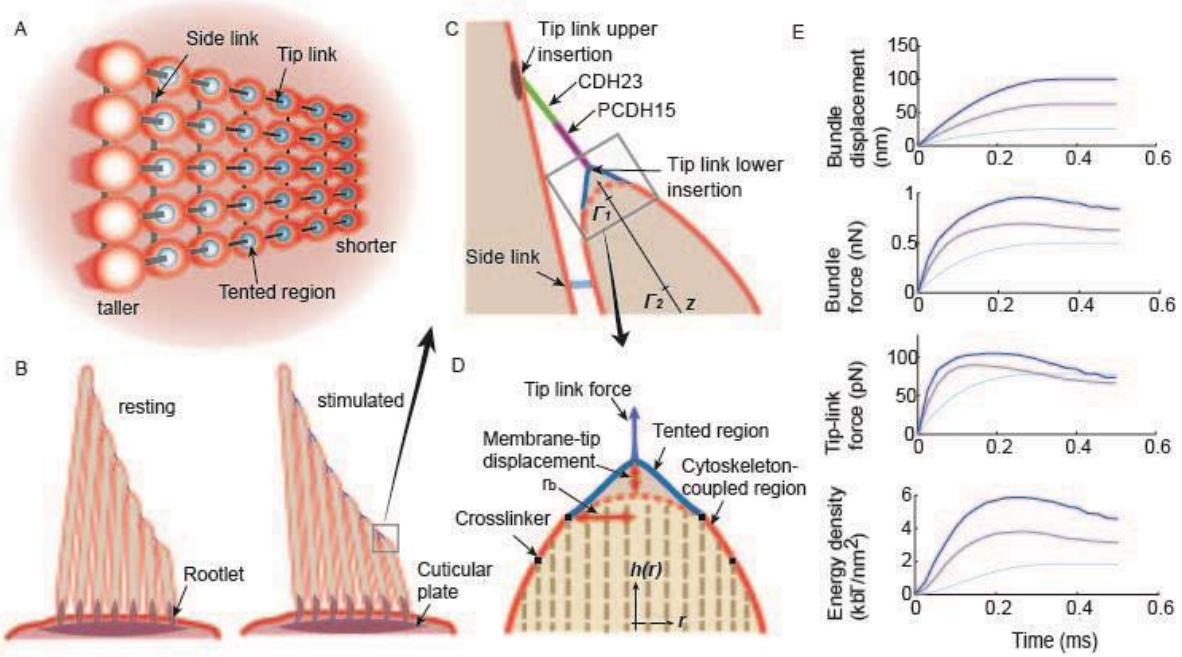

FIGURE 1 Description of the hair cell stereocilia bundle from turtle auditory papilla. (***A***) Top view for 5 rows and 7 column of stereocilia bundle inter connected by side and tip links. (***B***) Side view of the hair bundle provides the kinematic components in its resting (left) and stimulated (right) configuration. Stiff stereocilia bend about their base by deflecting rootlet. Side links ensure the bundle moves coherently while the tip link exerts force onto the membrane. (***C***) Ciliary tip and tip link complex. The tip link, composed of CDH23 and PCDH15, is inserted in the upper dense region while the other end is tethered into the lipid membrane. Membrane proteins presumably located in the tip region are not considered in this model. Tension on the tip link separates the membrane from the cytoskeleton. (***D***) Partitioned lipid membrane for the stereocilia tip. The red region could be tightly coupled to the stereocilia cytoskeleton (i.e. a bundle of actin filaments) through a crosslinker while the blue describes the membrane tented region where the tip link inserts. (***E***) Model responses to different size step functions (1st row) indicated with different intensity of blue. Bundle force (2nd row), single tip link force (3rd row), and membrane free energy density at a point 1nm from tip link lower insertion (4th row) are plotted. See Table 1 for the parameters used.

TABLE 1 Summary of the parameters. See SM Discussion for how these parameters are selected. (***A***) The value is varied from 0.2 to 0.05 fN/rad in Fig. 4A. (***B***) This value is varied from 17 to 30 nm in Figs. 2 and 4B.

Material properties	**Selected values**
Φ_0 (resting lipid areal density)	$1000/629 \times 10^{18}$ $/m^2$
σ_0 (lipid bilayer surface tension with zero density strain)	exp(-7) *mN/m*
k_m (lipid bilayer bending modulus)	$36k_bT$
K_{app} (lipid bilayer apparent area stretching modulus)	300 *mN/m*
$k_{rootlet}$ (rootlet rotational stiffness of single stereocilium)	0.2 fN/rad [(A)]
D (lipid diffusion constant)	7 $\mu m^2/s$

$\Delta A_{channel}$ (hair cell MS channel area difference between open and closed states)	*3 nm*^{2}
Unknown Parameters	**Tested values**
ΔG (hair cell MS channel internal energy difference between open and closed states)	7 k_bT
r_b (radial size of axisymmetric membrane)	21nm (B)

Kinematics and mechanics of the hair bundle

In the hair bundle model, the actin core, tip links, and side links are modeled as rigid bodies (see Fig. 1). The side links are allowed to slide freely along the surface of the taller stereocilium in order to constrain a fixed distance between two adjacent stereocilia (9). The model contains two deformable components: the rotational elastic spring of the rootlet and the lipid bilayer membrane of each stereocilium. These two elements interact with the rigid-body components to yield the following equilibrium equation for a hair bundle row composed of seven stereocilia (see Fig. S2 for the free body diagram):

$$\begin{bmatrix} a_1\cos(\theta_1) & -c_1 & & & \\ & a_2\cos(\theta_2-\theta_1) & \ddots & & \\ & & \ddots & -c_6 & \\ & & & a_7\cos(\theta_7-\theta_6) & \end{bmatrix}\begin{bmatrix} F \\ F_{sl1} \\ \vdots \\ F_{sl6} \end{bmatrix} = \begin{bmatrix} k_1 & & \\ & \ddots & \\ & & k_7 \end{bmatrix}\begin{bmatrix} \theta_1-\theta_{1,init} \\ \vdots \\ \theta_7-\theta_{7,init} \end{bmatrix} - \begin{bmatrix} 0 & -b_1\cos(\pi/2-\alpha_1) & & & \\ & a_2\cos(\pi/2-\alpha_1+\theta_2-\theta_1) & \ddots & & \\ & & \ddots & -b_6\cos(\pi/2-\alpha_6) & \\ & & & a_7\cos(\pi/2-\alpha_6+\theta_7-\theta_6) & \end{bmatrix}\begin{bmatrix} 0 \\ f_{tl1} \\ \vdots \\ f_{tl6} \end{bmatrix} \quad [1]$$

Each stereocilium is identified with index *i*, with the shortest designated *i=1* and the tallest *i=7*. The coefficients a_i, b_i, and c_i correspond to the total stereocilium height, the height to the tip-link upper insertion site, and the height to the side-link sliding insertion point, respectively; θ_i is the cuticular plate to rootlet angle; α_i is the angle between the tip link and the stereocilium; f_{tli} is the force in the tip link connecting the *i* and *i+1* stereocilia; similarly, F_{sli} is the force in the side link connecting the *i* and *i+1* stereocilia; and *F* is the force applied to the tallest sterocilium. Expressing Eq. [1] in matrix form,

$$\bar{\mathrm{A}}\cdot\vec{F} = \vec{K}\cdot\vec{\theta} - \bar{\mathrm{B}}\cdot\vec{f}_{TL} \quad [2]$$

the components k_i of the diagonal matrix $\vec{K}$ represent the linear torsional stiffness of the stereociliary rootlets. In prescribing the motion of the hair bundle, the angles θ_i are determined from the kinematics of the bundle motion, from which the arrays $\vec{\theta}$, $\bar{\mathrm{A}}$, and $\bar{\mathrm{B}}$ can be determined. Eq. [2] can be solved for the vector $\vec{F}$, which includes the bundle row force *F*, as well as the internal forces F_{sli} in the six side links. Assuming five rows of stereocilia shown in Fig 1A, the total summed bundle force is then simply found from $F_{total} = 5F$.

Membrane deformation in the tented-tip region

The tip link force can be found by modeling the lipid bilayer membrane deformation

over the tip region. Given the axisymmetric geometry of the stereociliary tip, shown in Fig 1D, the total potential energy of the tented tip membrane is given by

$$\Pi_{total} = E_{tip-compartment} - W \quad [3]$$

where $E_{tip\text{-}compartment}$ is the membrane free energy and W is the external work. The membrane free energy can be written in a Canham-Helfrich form (11, 12, 19),

$$E_{tip-compartment} = \int \left(2k(H - H_0)^2 + k_g K + \sigma\right) dA \quad [4]$$

Using the Monge gauge, which employs the function *h(r)* to measure the height of the lipid membrane above a reference plane, and the radial coordinate *r* (Fig. 1D), the mean curvature *H* and Gaussian curvature *K* appearing in Eq. 4 can be expressed as

$$H = 0.5\left(\frac{h_{rr}}{\sqrt{1+h_r^2}^{\,3}} + \frac{h_r}{r\sqrt{1+h_r^2}}\right) \quad [5]$$

$$K = \frac{h_{rr}h_r}{r\left(1+h_r^2\right)^2} \quad [6]$$

First and second derivatives of the membrane height function *h(r)* are indicated by h_r and h_{rr}, respectively. In Eq. 4, H_0 denotes the spontaneous curvature of the membrane, which can be equivalent to the cytoskeleton curvature for the tip region, and $dA = 2\pi r\sqrt{(1+h_r^2)}dr$ is the membrane axisymmetric area element. The constants *k* and k_g in Eq. 4 are the bending modulus and Gaussian curvature modulus, respectively. For all values of tip link stimulus, changes in the Gaussian curvature energy integrated over the membrane surface are identically zero according to the Gauss-Bonet theorem (20).

An expression for the membrane surface tension σ for the tip membrane of uniform lipid density can be found from the vesicle in a pipet experiment as follows (21, 22).

$$\sigma = \sigma_0 \cdot \exp\left(\frac{8\pi k_m}{k_b T}\alpha\right) \quad for \quad \alpha \le \alpha_{cross} \quad [7]$$

$$\sigma = K_{app}\left(\alpha - \alpha_{cut}\right) \quad for \quad \alpha > \alpha_{cross}$$

Here, the cut-off strain α_{cut} and cross-over strain α_{cross} can be selected to have smooth continuity for two surface tension equations in Eq. 7 at α_{cross}. σ_0 is surface tension with zero strain and K_{app} is the apparent area stretching modulus. The vesicle area strain, or the lipid density strain, α is simply $\alpha = \phi_0/\phi - 1$, where ϕ and ϕ_0 are the stimulated and resting lipid number density (number of lipid molecules/area), respectively.

Noting that *h(0)* defines the membrane-tip displacement, the external work *W* of the tip-link force appearing in Eq. 3 is given by

$$W = f_{tl}\, h(0) \quad [8]$$

The equilibrium configuration, free energy, and free energy densities of the tented-tip membrane can be obtained by finding the stationary of the total potential energy given by Eq. 3 such that $d\Pi_{total} = dE_{tip-compartment} - dW = 0$. With the given prescribed membrane-tip displacement shown in Fig. 1D, this is equivalent to finding *h(r)* which satisfies $\delta E_{membrane} = 0$. From Eq. 8 it follows that the tip-link force is then given by $f_{tl} = \partial E_{tip-compartment}/\partial h(0)$ with respect to the equilibrated membrane configuration. Using Eq. 4, the total tip-link force may be decomposed into flexing and stretching contributions for the membrane deformation as $f_{tl} = f_{flexing} + f_{stretching}$. Here, flexing and stretching forces can be defined by $f_{flexing} = \partial\left(\int 2k(H-H_0)^2\, dA\right)/\partial h(0)$ and $f_{stretching} = \partial\left(\int \sigma\, dA\right)/\partial h(0)$,

respectively (see Fig. 3B for the tip-link force decomposition). The shape of the lipid membrane, given by the height function *h(r)*, is approximated by using a Fourier series expansion, and the membrane energy is then minimized with respect to the Fourier coefficients. At the junction where the tented-tip region joins the cytoskeleton-coupled membrane, the radius is denoted by $r = r_b$ and the tented-tip membrane height function *h(r)* is also constrained to be C^1-continuous with the cytoskeleton-coupled membrane. At the tip-link insertion site $r = 0$, and the height function is constrained to satisfy $h_r(0) = 0$, which is required by symmetry. In this model, $k_g = (1- \upsilon)k = 0.5k$ is assumed (23), where υ is the Poisson ratio of the lipid membrane.

Theory for the lipid flow in the stereocilia

The lipid flow in the cytoskeleton-coupled region modulates the lipid density in the tented-tip membrane, and the rate of transport depends on the mobility of lipids in the cytoskeleton-coupled region. Under action of tip-link pulling, the movement of the continuous membrane from the viscous skeleton-coupled region to the minimally viscous tip region can be controlled by two different kinds of physical flow of the lipid molecules in the cytoskeleton-coupled compartment (see illustration in Fig. S3 for the motion of lipids with different mobility).

First, the diffusive flow generated by Brownian motion of the lipid follows the lipid density gradient, and the diffusive flux of lipids can be modeled by using Fick's law as follows

$$J_{diffusion}(z,t) = -D \cdot L(z) \cdot \frac{\partial}{\partial s}\phi(z,t) \quad [9]$$

Here, the z-coordinate lies on the central axis of the cylindrically symmetric cytoskeleton-coupled region shown in Fig. 1C. The arc-length element is given by $ds = \sqrt{dz^2 + dr^2}$, where *r(z)* is the radius of the cylindrical stereocilia at z. The circumferential length of the cytoskeleton-coupled region at z is thus given by $L(z) = 2\pi r(z)$. The diffusion constant for the lipids in this region is denoted by *D* and $\phi(z, t)$ is the lipid number density, varying spatially with respect to *z* and temporally with respect to *t*.

The second component is the convectional flow of lipids. The term "convection" may remind us of the lipid movement due to the flow of the external media. In fact, most studies involving modeling of lipid convectional flow have dealt with a velocity field directly applied to the lipid membrane (24-26). However, the convectional velocity formulated here is driven by the change in the potential energy interaction among lipid molecules. In a cellular environment where the membrane is strongly interacting with the cytoskeleton, viscous shear drag and the corresponding non-uniform stretching of the membrane can be significant (13). As denoted in Fig. S4B, the possible crosslinking proteins anchored to the cytoskeleton may play a role like a picket against the flow of lipids and such interactions potentially generate non-uniform stretching of the membrane. The non-uniform stretching and the corresponding surface tension gradient may result in spatial variation of the convective velocity $\upsilon(s,t)$ of the lipid molecules. In the cytoskeleton-coupled region, the convective flux of the lipid is formulated as follows

$$J_{convection}(z,t) = L(s) \cdot \phi(s,t) \cdot \upsilon(s,t) = \frac{2D}{k_b T} L(z) \frac{\partial \sigma(z,t)}{\partial s} \quad [10]$$

where k_b is Boltzmann's constant and *T* is temperature in Kelvin. Here, the surface tension σ is a function of ϕ given by Eq. [7] (see SM Methods for the detailed formulation of Eq. 10). Quantitative analysis of the Eqs. 9 and 10 indicates that in most cases the convection has much greater contribution for the lipid flux whereas contribution from diffusion is minimal. Now, considering particle number conservation (i.e. balance law), the final equation for the lipid flow

and the corresponding lipid density profile in the cytoskeleton-coupled region of the stereocilia can be found from

$$\frac{\partial}{\partial t}\left(L(z)\cdot\phi(z,t)\right) = -\frac{\partial}{\partial s}\left(J_{diffusion}(z,t)+J_{convection}(z,t)\right) = D\frac{\partial}{\partial s}\left(L(z)\cdot\frac{\partial\phi(z,t)}{\partial s}-\frac{2}{k_bT}L(z)\cdot\frac{\partial\sigma(z,t)}{\partial s}\right) \quad [11]$$

The lower boundary of the membrane is defined by a plane with elevation given by $z=\Gamma_2$ ($z=\Gamma_2$ and $z=\Gamma_1$ are denoted in Fig. 1C). The boundary condition imposed on ϕ at this plane corresponds to a constant resting lipid density

$$\phi(\Gamma_2,t)=\phi_0 \quad [12]$$

This boundary condition corresponds to an infinite supply of lipid molecules at fixed number density. The upper coupled region boundary is located at the interface with the tented-tip region at $z = \Gamma_1$. The boundary condition imposed here describes a balance of lipid flux at the interface to the time rate of change of the total number of lipid molecules in the tented tip,

$$J_{diffusion}(\Gamma_1,t)+J_{convection}(\Gamma_1,t)=-\frac{\partial}{\partial t}\left(\phi_{tip}\cdot A_{tip}\right) \quad [13]$$

where A_{tip} is the area of the tented-tip membrane. This boundary condition implies that lipids supplied from the cytoskeleton-coupled region to the tip region instantaneously reorganize the inter-lipid distance to produce a uniform lipid density over the tip (see Fig. S3). When the membrane is not pulled, the resting lipid density is initially uniform (i.e. $\phi\ (z,\ t=0)=\phi_0$). The lipid transport model presented in this study is implemented numerically by using a finite-difference scheme.

Probability of opening the channel

The possibility that the membrane free-energy density in the tip region can be used to determine the opening of the mechanotransduction channel is also explored. The total potential energy of a virtual channel E, including the applied external load from the lipid membrane to the channel, $F_\rho\Delta A_{channel}$, can be written as:

$$E(\lambda,\tau)=(1-\lambda)G_{closed}+\lambda G_{open}-\lambda F_\rho\Delta A_{channel} \quad [14]$$

The free-energy density of the tip membrane F_ρ can be expressed directly using the integrands in the Helfrich form of Eq. 4 when the membrane is equilibrated. The two-state variable λ represents either the open ($\lambda=1$) or closed ($\lambda=0$) configuration of the channel. G_{open} and G_{closed} represent the internal energy of the channel for open and closed configurations, respectively. The energy required for the channel to open is calculated as the product of the membrane free energy density and the area difference $\Delta A_{channel}$ between the open and closed configurations of the mechanotransduction channel, and is subtracted from the total potential energy when the channel is open. Given the total potential energy of the channel expressed in Eq. 14, a Boltzmann distribution can be defined to determine the probability of finding the system in a state with total channel energy E, which results in the following probability function for the channel opening (27):

$$p=\frac{1}{1+\exp\left(\frac{1}{k_bT}\left(G_{open}-G_{closed}-\tau\Delta A_{channel}\right)\right)} \quad [15]$$

where G_{open}-G_{closed}=ΔG and $\Delta A_{channel}$ are treated as constant channel parameters.

RESULTS

Time dependent responses to step displacements

Temporal responses generated by the model to a series of displacement steps to the tallest stereocilium are presented in Fig. 1E. Plotted against time are the bundle force, whose value is a function of the summed stereocilia response, the single tip link force, and the membrane free energy density calculated at a point 1 *nm* from the tip link insertion site. Force applied both at the tip link and across the bundle has a rapid onset and is graded with intensity. Responses are complex temporally, with a decrease in force observed during a continued stimulation. Such force relaxation is generated by the lipid flow for the non-uniformly stretched membrane to homogenize the lipid area density. As the focus is on the force vs. displacement relationship, temporal changes are less consequential; however they do demonstrate that lipid energy is accumulated fast enough to be relevant to hair cell activation. Calculations are sampled at *0.5 ms* from the onset of the stimulation to plot force and energy vs. displacement relationships to mimic previous experimental data from a turtle (4).

Role of the lipid mobility and size of the tented region

The main variables associated with the membrane deformation are the radial size of the tented-tip region, and the lipid mobility in the cytoskeleton-coupled region. To investigate the relative contribution of these variables, each variable is systematically varied. The radius of the tented-tip region r_b is stepped through 17, 21, and 30 *nm* and the lipid mobility for the cytoskeleton-coupled region, parameterized by the diffusion constant D, is set to be hypermobile (i.e. $D \rightarrow \infty$) and D=7 $\mu m^2/s$ (see Fig. S3 for description of the lipid mobility). The hypermobile case can be solved without considering time dependency and the force vs. displacement result is obtained with a quasi-static analysis. The cases with physiologically relevant diffusivity values, i.e. D=7 $\mu m^2/s$, are solved by sampling the calculation in the temporal step response, as depicted previously; data between sample points are linearly interpolated. Plots of membrane-tip displacement vs. tip-link force and membrane free energy density 1 *nm* from the tip-link insertion are presented in Figs. 2A and B, respectively.

The characteristic nonlinearity of the tip link force vs. membrane-tip displacement relation can be altered by varying the values of both the radius of the tip region r_b and the lipid diffusion constant D (Fig. 2A). In Fig. 2A, the negative stiffness in the regime where the force is reduced (around the membrane-tip displacement of 18 *nm*) is strongly dependent on the membrane radius r_b; smaller values of r_b result in greater negative stiffness. On the other hand, the ability of the tip link force to be increased with larger displacements is strongly dependent on the lipid mobility in the cytoskeleton-coupled region. For a given value of r_b, the tip link force on the larger displacement increases with a reduction in the lipid mobility from hypermobile to the physiologically relevant value. In Fig. 2A with r_b=21nm and D=7 $\mu m^2/s$, the nonlinear characteristic showing minimum stiffness in the intermediate displacement is very similar to that of the measured hair bundle nonlinearity (3-5).

In Fig. 2B the free energy density of the membrane at 1 *nm* shows similar trends as the tip link force, but monotonically increases when D=7 $\mu m^2/s$, while the tip link force does not. It is unlikely that channel activation is directly following the tip link force because hair cell activation curves do not activate less with larger stimulation. In this perspective, it would be reasonable to assume that channel activation follows the membrane energy. To further explore

the membrane free energy in channel activation, a plot of the free energy density profile for the tented-tip region at 0.5 *ms* when the bundle is step displaced with 50 *nm* (corresponding to the data indicated by the blue arrow in Fig. 2B, middle panel) is presented in Fig. 2C. The free energy density rapidly decays from the tip link insertion site. One might also predict that the free energy would also increase minimally at the interface between two compartments due to increased curvature (see arrow in Fig. 2C). The profile suggests that if the free energy associated with membrane deformation induced by the tip link force is used to activate the MS channel, then the channel should be located close to the tip link insertion site for efficient energy transfer.

The free energy density of the membrane surface associated with tip link displacement consists of mean and Gaussian curvature energies and surface tension energy, according to the Helfrich theory (see Eq. 4). These three energy densities correspond to the calculated data in Fig. 2B indicated by the middle blue trace and are shown separately in Fig. 2D. As seen in Fig. 2D, the two curvature energy densities are dominant while the surface tension energy density is negligible. The mean and Gaussian curvature energy densities have the same order of magnitude and either or together could potentially be sufficient to activate the MS ion channel of the hair cell. Assuming the channel gating is sensitive to the mean curvature energy, with the energy difference between open and closed states being $7k_bT$, the mean curvature energy density sampled at 1 *nm* from the tip link generates the activation curve in Fig. 2E. Here selection of the channel energy $7k_bT$ might be arbitrary for the hair cell MS channel as the structural identity of the channel remains unknown. However, a typical MS channel has an internal energy difference of $\sim 10k_bT$ between open and closed states (27), and the hair cell channel energy is also estimated as $\sim 10k_bT$, although the theoretical of the present model is different (28). The channel open probability analysis presented here indicates that potentially enough energy required for the channel to open is present, and that the channel needs to be close to the tip link to sense enough lipid membrane energy for effective activation. This proximity is consistent with the channel being linked in some manner to the tip link in consideration of the fluid nature of the lipid membrane. Perhaps the recent hypothesis that the TMHS protein serves as a linker between the MS channel and the tip link provides a molecular underpinning to this idea where TMHS keeps the channel in the sensitive portion of the membrane (29).

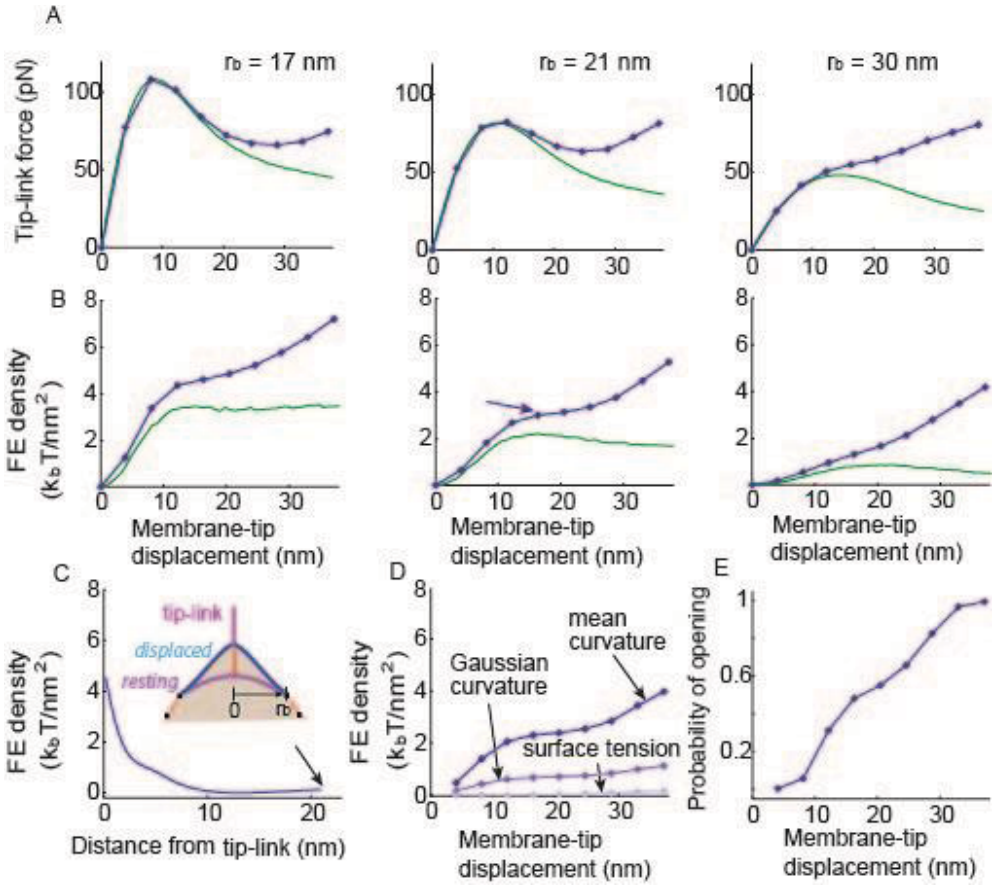

FIGURE 2 Effects of varying lipid mobility and r_b for the membrane (***A***) Tip link force and (***B***) membrane free energy density at a point 1 nm from the tip link insertion site (i.e. r = 1 *nm*) with respect to membrane-tip displacement. Both responses are obtained at time=0.5 *ms* from the step stimuli stimulation shown in Fig. 1E. Data are indicated with linearly interpolated dots for D=7 $\mu m^2/s$ case (blue). Hypermobility (green) of the lipid in the cytoskeleton-coupled region is also considered in (*A*) and (*B*). 1st, 2nd, and 3rd columns of (*A*) and (*B*) use r_b=*17 nm, 21 nm*, and *30 nm*, respectively. (***C***) Free energy density profile of the tented-tip membrane corresponding to the arrowed data in (*B*), middle panel (r_b=*21 nm*). (***D***) Decomposed membrane free energy density shown with a blue trace in (*B*), middle panel. (***E***) Open probability of the imaginary MS channel using free energy density contribution from mean curvature (i.e. highest contribution among three different energy density sources in (*D*)). See Table 1 for the parameters used.

Nonlinear force vs. displacement relationship for hair bundle

To determine whether deformation of the membrane could actually reproduce the nonlinear bundle force vs. displacement response, the total bundle force is computed for the hypermobile and D= 7 $\mu m^2/s$ conditions in Fig. 3A. Nonlinear responses are obtained with each condition. However, the results again reveal that using limited lipid mobility in the cytoskeleton-coupled region is the key to increasing the bundle force in the large displacement regime, and thus to have a more similar curve shape with nonlinear bundle force measurements. Similar to the experimental data, loss of tip links linearizes and reduces the hair bundle force. Loss of the side links further reduces the linear force, by terminating coherent coordinated movement of the bundle.

For the condition where the lipid mobility of the cytoskeleton-coupled region is limited to the physiologically relevant value (Fig. 3B, upper panel), or where they are hypermobile (Fig. 3B, lower panel), the single tip link force is decomposed into two different force contributions to better interpret the underlying physical mechanism of this nonlinearity. Here two decomposed tip-link forces are termed the flexing force and stretching force: the flexing force component is responsible for changing the curvature of the tented membrane; and the stretching force component is responsible for the increased area of the tented membrane (see Method section for the mathematical definition of flexing and stretching forces). In both cases, the nonlinear flexing force increases sharply with onset of displacement. For larger displacements, the flexing force is reduced after its peak value by showing a saturation characteristic. The stretching force is most sensitive to the lipid mobility in the cytoskeleton-coupled partition. When the hypermobility is defined for the cytoskeleton-coupled region stretching force is negligible, but a significant amount of stretching force exponentially increases when the physiologically relevant limited mobility of the lipid is used. This increased stretching force can be explained by the following: the increased membrane area must accompany an increase of the lipid-to-lipid distance when the membrane-to-skeleton viscosity is considered whereas it does not when the system is hypermobile. Therefore, defining the viscous membrane system is the key to generating a more complicated nonlinear force vs. displacement response that is more similar with experimental measurements.

After seeing that the exponentially increased stretching force restores the total tip link force in the larger displacement regime in the upper panel of Fig 3B, understanding the behavior of the nonlinear flexing force, which is decayed and saturated after its peak, appears to be critical to interpret the biophysical mechanism of the bundle nonlinearity. The reduced flexing force calculated here can be postulated to occur at the point where the maximum curvature change is reached, although the membrane tip is continuously pulled away from the cytoskeleton core. More specifically, despite the continuously increasing membrane-tip displacement, the curvature near the point source of the tip link and the boundary of the two membrane partitions is saturated. Therefore, based on a mechanism similar to the “lever principle”, force driving the curvature of the membrane (i.e. flexing force) might be decreased.

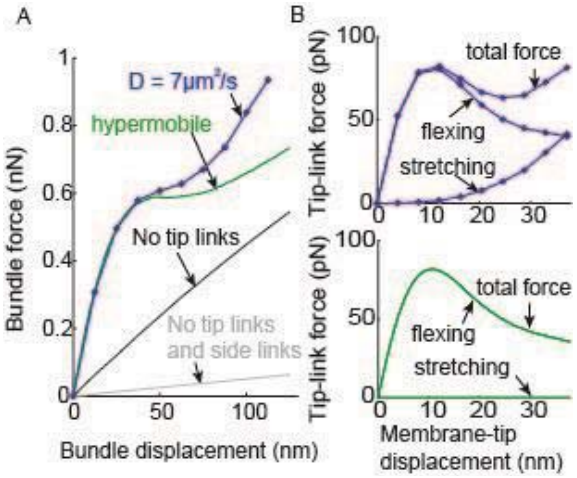

FIGURE 3 Bundle force vs. displacement responses and tip-link force decomposition (***A***) Force vs. displacement responses for the 5 rows of the 7 staircase pattern stereocilia coupled with 6 tip links and 6 side links (shown in Fig. 1A). From the tip-link force vs. membrane-tip displacement

response in the middle panel of Fig. 2A (r_b=*21nm*), bundle force vs. displacement responses are plotted. Two different mobilities of the lipid in the cytoskeleton-coupled region (blue for $D=7\mu m^2/s$ and green for hypermobile lipid) are considered. Detachment of the tip links from the membrane linearized the response (black), and disconnecting side links as well further reduce the magnitude of the linear response (gray). (***B***) Membrane flexing and stretching components of the tip-link force. For each case of lipid mobility, the total single tip-link force is decomposed into two different force contributions (see Methods section for the mathematical definition of the forces). See Table 1 for the parameters used.

In frog saccule hair bundles, force vs. displacement measurements often have a negative slope (30). This negative stiffness potentially identifies a mechanical amplification mechanism and thus understanding the underlying mechanism for its generation is relevant (30). The model results show that the magnitude of the nonlinearity observed in the force vs. displacement plot is in part dictated by the choice of rootlet stiffness. As shown in Fig. 4A, decreasing the rootlet stiffness generated a negative slope, similar to that observed in the frog (30). Bundle stiffness vs. displacement plots are also presented to further illustrate the negative stiffness. Single rootlet stiffness measurement for the frog is not available, but comparison of the whole bundle stiffness calculation with $k_{rootlet}$=0.05 *fN/rad* (Fig. 4A) to the whole bundle frog measurement shows good agreement. Whether this is biologically relevant remains to be explored but it does offer an alternative explanation for the negative stiffness and a rationale for why this phenomenon has only been observed in the frog saccule where the rootlets are more compliant, and not in turtle or mammalian preparations

The nonlinearity in force vs. displacement measurements can be abolished with treatment of a drug during the hair cell preparation. In this experiment, the drug treatment also results in blockage of the transduction current when a hair bundle is stimulated (3). In the original gating spring model, such observations provide a causal link between channel activation and the nonlinear bundle mechanics under the simple assumption that the drug bonds to the channel protein and prohibits the opening of the channel (3). However, recent data on treatment of aminoglycosides to block the transduction current and to abolish nonlinear bundle mechanics demonstrate that aminoglycosides are permeable to this channel to the cytoplasm of the stereocilia tip and thus it is unlikely that they can bind to a particular position of the channel (31, 32). So how does blocking mechanotransducer current then interfere with nonlinear mechanics? In the present model, the force vs. displacement response is linearized by simply increasing r_b. That is, by increasing the radial size of the tented-tip region to 30 *nm* from 17 *nm*, the nonlinearity is lost (Fig. 4B) and the channel open probability is also reduced by following the reduction of the membrane free energy density. The results may suggest mechanisms by which the size of the tented-tip region can be controlled by a certain intracellular mechanism generated by aminoglycoside treatments. Although the validity of this model prediction must still be tested, it nonetheless provides an alternative explanation for the mismatch between the classical hypothesis and the recently measured data.

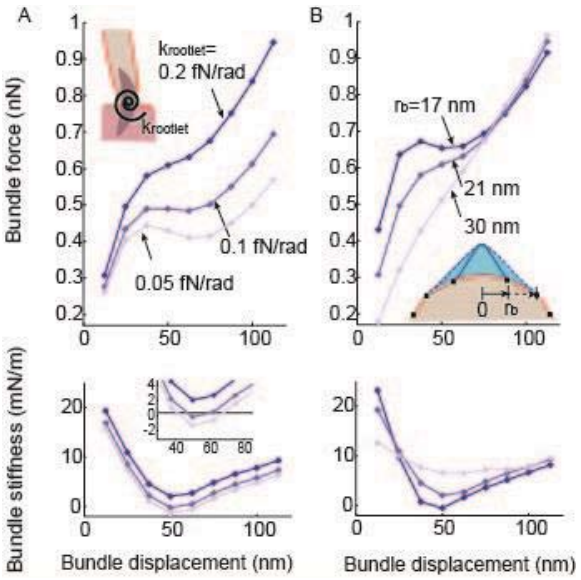

FIGURE 4 Possible mechanisms for the negative stiffness and the linearization component. Using bundle force vs. displacement response with $D=7\ \mu m^2/s$ in Fig. 3A, force (top) and stiffness (bottom), responses are calculated by varying the rotational stiffness of the rootlet, and the parameter r_b. (***A***) Generation of the negative bundle stiffness by decreasing the stiffness of the rootlet (with fixed r_b=21*nm*). (***B***) Linearized bundle force responses by increasing r_b (with fixed $k_{rootlet}$=0.2*fN/rad*). See Table 1 for the parameters used.

Although a nonlinear calculation similar to the measurement is achieved in Fig. 3A, as it stands the model does not directly reproduce the biological nonlinearity measured in the turtle hair bundles. The nonlinear force vs. displacement calculation (0 *nm* case in Fig. 5B, which correspond to $D=7\ \mu m^2/s$ in Fig.3A) is shifted as compared to actual measurements (Ricci et al. in Fig. 5B). In order to align the model results with the measured data, it is necessary to apply a standing tip link force in the resting configuration of the hair bundle. This standing force, as depicted in Fig. 5A, is posited to be contributed by the forces exerted at the upper tip link insertion, perhaps due to myosin motor proteins, as suggested for adaptation processes (33, 34). A standing membrane-tip displacement of 5.6 *nm* resulting in a standing force of about 50pN is sufficient to reproduce the data obtained from turtle auditory hair cells (4). This standing tip-link force is similar with that of mammalian (~60 pN) but greater than that of frog saccule hair bundles (35, 36). With this standing tension in place, disruption of the tip link resulted in a hair bundle movement toward the tall edge as has been previously reported (37).

To illustrate that the membrane energy can serve to activate the hair cell MS channel and that the channel activation follows the nonlinear force vs. displacement plots, again an imaginary channel sensitive to the mean curvature energy of the membrane and the channel internal energy difference between the opened and closed state of $7k_bT$ is assumed at a 1 *nm* point from the tip link. Activation curves are generated and presented in Fig. 5D. The plots are presented for different standing tip link tensions to demonstrate that channel activation shifts in parallel with the nonlinear force vs. displacement plot overlap the minimum stiffness region in the force plot and the half open probability region in the activation curve, as previously shown experimentally (3, 4). In this model, however, different from previous interpretations, the nonlinearity is not causally linked to channel activation as the channel is passively following the membrane energy.

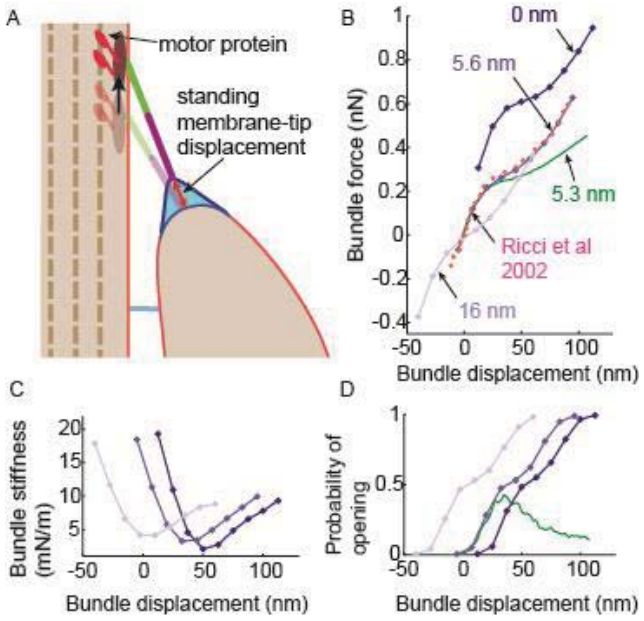

FIGURE 5 Standing membrane-tip displacement and corresponding migration of the bundle force vs. displacement responses. (***A***) Schematic representing a possible mechanism of applying a standing force to the tip link using a motor protein at the upper insertion point. (***B***) Hair bundle force vs. displacement plots with varying levels of the standing membrane-tip displacement (blue affiliation), using $D=7\ \mu m^2/s$ from Fig. 3A. The calculation correlating best with experimental data (magenta, Ricci et al. 2002) uses a standing membrane-tip displacement of 5.6 nm. The zero displacement corresponds to zero bundle force for all cases in (*B*). (**C**) Bundle stiffness calculated from (B). (***D***) Open probability of the imaginary MS channel calculated using the membrane mean curvature free energy density at a point 1 nm from the tip link insertion site. Here, the half channel opening probability region ($P=0.5$) in (*D*) covaries with the minimum stiffness region of the force vs. displacement response in (*B*) in response to the different magnitude of the standing tip-link force. The hypermobile case (green) demonstrates that neither nonlinear force vs. displacement in (*B*) nor open probability of the channel in (*D*) can be explained when the lipid mobility in the cytoskeleton-coupled region is not physiologically relevant. See Table 1 for the parameters used.

DISCUSSION

Prevalent in many end organs and species, the nonlinear force vs. displacement relationship can be seen in auditory hair bundles in activating the mechanosensitive (MS) ion channels of sensory hair cells. However, the underlying biophysical mechanism of this nonlinearity and the channel activation has remained elusive (3-5, 38). Here, a theoretical framework in which the lipid membrane deformation explains the bundle nonlinear force vs. displacement measurement is presented. In this model, two partitioned lipid membranes, a small component that can be separated from the actin core (i.e. the tented-tip region) and a pool where the curvature change is not considered (i.e. cytoskeleton-coupled region), define the stereocilia lipid membrane. Here, lipid mobility in the tented-tip region is fast enough to be quasi-static while it is significantly limited in the cytoskeleton-coupled region. When the bundle is deflected, forces applied at the tip link generate a rapid membrane flexing component of the tip-link force.

Larger stimulations reduce the flexing force component but increase the stretching force due to the decreased lipid area density under viscoelastic interactions. When nonlinearity occurs, the stretching force does not compensate for the reduced flexing force and results in an overall reduction in the force, whereas the stretching force restores the total tip link force at still larger displacement.

The model suggests that the membrane curvature change can generate the energy needed to activate the MS channels of the hair cells. Although this ability of the lipid to convey force is less understood for hair cells mechanostrasduction, it is a much more accepted phenomenon across other mechanoreceptors. For instance, the MscL and MscS channels use the energy created by the lipid to control the turgor pressure of bacterial (39-41). Many other mechanosensitive ion channel including TREK-1, TRAAK, PIEZO-1 and -2 channels are all sensitive to the lipid membrane stretching (42-48). The model suggests that the force applied to the channel may have a more common underpinning to other mechano-sensory systems and that the nonlinearity of the hair cell system might be generated by the cellular and molecular environment of the stereocilia effectively controlling this force transfer to the channel. Recent modeling works where the membrane tenting is similarly investigated also support the force conveying role of the lipid for auditory mechanotransduction (49, 50). However, mechanism for the nonlinear force vs. displacement measurements still remains elusive in these works.

A caveat in exploring how the lipid membrane stretches is the possibility that the membrane might be able to rupture. The rupture parameters estimated from vesicles indicate that a decrease of about 3-5% in lipid density may lead to rupture of the lipid membrane. However, in this model simulation with consideration of the physiologically relevant diffusion constant, it turns out that the membrane density strain does not increase to a value above 3% with any tested rise time of the bundle in the step stimuli; for all data presented in this paper, the maximum lipid density strains are less than 1%. Such a low density strain despite significant area generation can be achieved by the fast convective flow of the lipid followed by the membrane surface-tension gradient (see method section for the formulation of convective flow of lipids). Of course, unreasonably fast stimulation of the bundle or assuming critically limited lipid mobility in the cytoskeleton-coupled region can result in rupture of the lipid membrane, but in most cases of the bundle stimuli in real physiological conditions, stereocilia lipid membranes may not be stretched beyond the rupture point. It is also possible that transmembrane protein structures such as TMCs and TMHS molecules which interact with the tip link provide additional membrane support that would alter the ultimate rupture point (29, 51).

At present, without consideration of the channel protein, the energy decay gradient near the tip link insertion site is quite steep (Fig. 2C). This steepness is in part influenced by the point source nature of the stimulus. However, if stiffer trans-membrane elements such as an ion channel are inserted near the tip link insertion, then the energy density profile can be changed to show a very small gradient with a high magnitude near the tip link insertion site; and a steep gradient generated at the region away from the tip link insertion site by the size of the channel. However, shifting of the steep energy gradient region due to the addition of the channel would not change the nature of the membrane tenting problem; the sharp membrane curvature generation around the channel and boundary of the two membrane partitions remains, and also the lipid density still decreases. Therefore, adding the channel protein may not affect the major analysis regarding the nonlinear force vs. displacement relationship. This possibility is simulated with the assumption of a rigid disk at the center of the tip membrane and results are presented in Supporting Material Fig. S5. This simple analysis does not fully elucidate the effect of the

channel but at least demonstrates that the nonlinear force and the membrane energy density potentially sufficient to activate the channel also can be generated with the stiff membrane protein at the tip link lower insertion. It is also possible that the stimulation is not a point source but rather is introduced via multiple points, as the tip link has at least three independent insertion sites (10). Regardless, structural information for the hair cell MS channel is required to fully understand possible role of the channel for mechanotransduction, mechanics of the tented membrane, and overall bundle mechanics.

In summary, a theoretical framework that considers physical characteristics of the partitioned lipid membrane in the stereocilia is introduced. The model considers the membrane-cytoskeleton interaction and the corresponding viscous flow of the lipid and elastic deformation of the membrane under action of the tip-link pulling. The model reproduces biologically relevant hair bundle force vs. displacement responses by interpreting how bending and stretching of the membrane generate nonlinear tip-link force and by demonstrating the need for a resting tip-link tension. In addition, the model reproduces and predicts the mechanism for the negative stiffness as well as identifies a means by which nonlinearity could be lost (i.e. linearization component). This model also provides an energetic rationale for the channel that must be very close to the tip link. Overall, the theoretical analysis presented here suggests that the auditory mechanotransduction also can be delineated by the force conveying role of the lipid membrane – a unifying hypothesis for cellular mechanotransduction.

ACKNOWLEDGEMENTS

The author sincerely appreciates Dr. Peter M. Pinsky and Dr. Charles R. Steele at Stanford University for invaluable advisory inputs on modeling. The author also thanks Dr. Anthony Ricci and Dr. Sunil Puria at Stanford for supportive comments and discussion. Work was funded by Timoshenko fund from Mechanical Engineering Department at Stanford, NIH NIDCD grants RO1 DC007910 and RO1 DC003896.

REFERENCES

1. Peng, A. W., F. T. Salles, B. Pan, and A. J. Ricci. 2011. Integrating the biophysical and molecular mechanisms of auditory hair cell mechanotransduction. Nature communications 2:523.
2. Beurg, M., R. Fettiplace, J.-H. Nam, and A. J. Ricci. 2009. Localization of inner hair cell mechanotransducer channels using high-speed calcium imaging. Nature Neuroscience 12:553-558.
3. Howard, J., and A. Hudspeth. 1988. Compliance of the hair bundle associated with gating of mechanoelectrical transduction channels in the bullfrog's saccular hair cell. Neuron 1:189-199.
4. Ricci, A., A. Crawford, and R. Fettiplace. 2002. Mechanisms of active hair bundle motion in auditory hair cells. The Journal of Neuroscience 22:44-52.
5. Russell, I., M. Kossl, and G. Richardson. 1992. Nonlinear mechanical responses of mouse cochlear hair bundles. Proceedings of the Royal Society of London. Series B: Biological Sciences 250:217-227.
6. Hudspeth, A. 2008. Making an effort to listen: mechanical amplification in the ear. Neuron

59:530-545.

7. Kozlov, A. S., T. Risler, and A. Hudspeth. 2006. Coherent motion of stereocilia assures the concerted gating of hair-cell transduction channels. Nature Neuroscience 10:87-92.
8. LeBoeuf, A. C., D. Ó Maoiléidigh, and A. Hudspeth. 2011. Divalent Counterions Tether Membrane-Bound Carbohydrates To Promote the Cohesion of Auditory Hair Bundles. Biophysical journal 101:1316-1325.
9. Karavitaki, K. D., and D. P. Corey. 2010. Sliding adhesion confers coherent motion to hair cell stereocilia and parallel gating to transduction channels. The Journal of Neuroscience 30:9051-9063.
10. Kachar, B., M. Parakkal, M. Kurc, Y.-d. Zhao, and P. G. Gillespie. 2000. High-resolution structure of hair-cell tip links. Proceedings of the National Academy of Sciences 97:13336-13341.
11. Canham, P. B. 1970. The minimum energy of bending as a possible explanation of the biconcave shape of the human red blood cell. Journal of Theoretical Biology 26:61-81.
12. Helfrich, W. 1973. Elastic properties of lipid bilayers: theory and possible experiments. Zeitschrift für Naturforschung. Teil C: Biochemie, Biophysik, Biologie, Virologie 28:693.
13. Kusumi, A., C. Nakada, K. Ritchie, K. Murase, K. Suzuki, H. Murakoshi, R. S. Kasai, J. Kondo, and T. Fujiwara. 2005. Paradigm shift of the plasma membrane concept from the two-dimensional continuum fluid to the partitioned fluid: high-speed single-molecule tracking of membrane molecules. Annu. Rev. Biophys. Biomol. Struct. 34:351-378.
14. Furness, D., Y. Katori, B. Nirmal Kumar, and C. Hackney. 2008. The dimensions and structural attachments of tip links in mammalian cochlear hair cells and the effects of exposure to different levels of extracellular calcium. Neuroscience 154:10-21.
15. Sakaguchi, H., J. Tokita, U. Müller, and B. Kachar. 2009. Tip links in hair cells: molecular composition and role in hearing loss. Current opinion in otolaryngology & head and neck surgery 17:388.
16. Corey, D. P. 2009. Cell biology of mechanotransduction in inner-ear hair cells.
17. Schneider, M. E., A. C. Dosé, F. T. Salles, W. Chang, F. L. Erickson, B. Burnside, and B. Kachar. 2006. A new compartment at stereocilia tips defined by spatial and temporal patterns of myosin IIIa expression. The Journal of Neuroscience 26:10243-10252.
18. Zhao, H., D. E. Williams, J.-B. Shin, B. Brügger, and P. G. Gillespie. 2012. Large membrane domains in hair bundles specify spatially constricted radixin activation. The Journal of Neuroscience 32:4600-4609.
19. Brown, F. L. 2008. Elastic modeling of biomembranes and lipid bilayers. Annu. Rev. Phys. Chem. 59:685-712.
20. Powers, T. R., G. Huber, and R. E. Goldstein. 2002. Fluid-membrane tethers: Minimal surfaces and elastic boundary layers. Physical Review E 65:041901.
21. Evans, E., and W. Rawicz. 1990. Entropy-driven tension and bending elasticity in condensed-

fluid membranes. Physical Review Letters 64:2094.

22. Rawicz, W., K. Olbrich, T. McIntosh, D. Needham, and E. Evans. 2000. Effect of chain length and unsaturation on elasticity of lipid bilayers. Biophysical journal 79:328-339.
23. Hu, M., J. J. Briguglio, and M. Deserno. 2012. Determining the Gaussian curvature modulus of lipid membranes in simulations. Biophysical journal 102:1403-1410.
24. Hughes, B., B. Pailthorpe, and L. White. 1981. Translational and Rotational Drag on a Cylinder Moving in a Membrane. Journal of Fluid Mechanics 110:349-372.
25. Hochmuth, R. 1982. Solid and liquid behavior of red cell membrane. Annual review of biophysics and bioengineering 11:43-55.
26. Jiang, H. 2012. Dynamic Sorting of Lipids and Proteins in Multicomponent Membranes. Physical Review Letters 109:198101.
27. Ursell, T., J. Kondev, D. Reeves, P. A. Wiggins, and R. RobPhillips. 2008. Role of lipid bilayer mechanics in mechanosensation. In Mechanosensitive Ion Channels. Springer. 37-70.
28. van Netten, S. M., and C. J. Kros. 2000. Gating energies and forces of the mammalian hair cell transducer channel and related hair bundle mechanics. Proceedings of the Royal Society of London. Series B: Biological Sciences 267:1915-1923.
29. Xiong, W., N. Grillet, H. M. Elledge, T. F. Wagner, B. Zhao, K. R. Johnson, P. Kazmierczak, and U. Müller. 2012. TMHS is an integral component of the mechanotransduction machinery of cochlear hair cells. Cell 151:1283-1295.
30. Martin, P., A. Mehta, and A. Hudspeth. 2000. Negative hair-bundle stiffness betrays a mechanism for mechanical amplification by the hair cell. Proceedings of the National Academy of Sciences 97:12026-12031.
31. Pan, B., J. Waguespack, M. E. Schnee, C. LeBlanc, and A. J. Ricci. 2012. Permeation properties of the hair cell mechanotransducer channel provide insight into its molecular structure. Journal of neurophysiology 107:2408-2420.
32. Marcotti, W., S. M. Van Netten, and C. J. Kros. 2005. The aminoglycoside antibiotic dihydrostreptomycin rapidly enters mouse outer hair cells through the mechano-electrical transducer channels. The Journal of physiology 567:505-521.
33. Gillespie, P. G., and J. L. Cyr. 2004. Myosin-1c, the hair cell's adaptation motor. Annu. Rev. Physiol. 66:521-545.
34. Grati, M. h., and B. Kachar. 2011. Myosin VIIa and sans localization at stereocilia upper tip-link density implicates these Usher syndrome proteins in mechanotransduction. Proceedings of the National Academy of Sciences 108:11476-11481.
35. LeMasurier, M., and P. G. Gillespie. 2005. Hair-cell mechanotransduction and cochlear amplification. Neuron 48:403-415.
36. Jaramillo, F., and A. Hudspeth. 1993. Displacement-clamp measurement of the forces exerted by gating springs in the hair bundle. Proceedings of the National Academy of Sciences

90:1330-1334.

37. Assad, J. A., G. M. Shepherd, and D. P. Corey. 1991. Tip-link integrity and mechanical transduction in vertebrate hair cells. Neuron 7:985-994.
38. Markin, V. S., and A. Hudspeth. 1995. Gating-spring models of mechanoelectrical transduction by hair cells of the internal ear. Annual Review of Biophysics and Biomolecular Structure 24:59-83.
39. Anishkin, A., and S. Sukharev. 2009. State-stabilizing interactions in bacterial mechanosensitive channel gating and adaptation. Journal of Biological Chemistry 284:19153-19157.
40. Sukharev, S., and A. Anishkin. 2004. Mechanosensitive channels: what can we learn from 'simple'model systems? Trends in neurosciences 27:345-351.
41. Kung, C., B. Martinac, and S. Sukharev. 2010. Mechanosensitive channels in microbes. Annual review of microbiology 64:313-329.
42. Maingret, F., M. Fosset, F. Lesage, M. Lazdunski, and E. Honoré. 1999. TRAAK is a mammalian neuronal mechano-gated K+ channel. Journal of Biological Chemistry 274:1381-1387.
43. Patel, A. J., M. Lazdunski, and E. Honoré. 2001. Lipid and mechano-gated 2P domain K< sup>+</sup> channels. Current opinion in cell biology 13:422-428.
44. Sachs, F. 2010. Stretch-activated ion channels: What are they? Physiology 25:50-56.
45. Gottlieb, P. A., C. Bae, and F. Sachs. 2012. Gating the mechanical channel Piezo1: A comparison between whole-cell and patch recording. Channels 6:282-289.
46. Hua, S. Z., P. A. Gottlieb, J. Heo, and F. Sachs. 2010. A mechanosensitive ion channel regulating cell volume. American Journal of Physiology-Cell Physiology 298:C1424-C1430.
47. Coste, B., J. Mathur, M. Schmidt, T. J. Earley, S. Ranade, M. J. Petrus, A. E. Dubin, and A. Patapoutian. 2010. Piezo1 and Piezo2 are essential components of distinct mechanically activated cation channels. Science 330:55-60.
48. Coste, B., B. Xiao, J. S. Santos, R. Syeda, J. Grandl, K. S. Spencer, S. E. Kim, M. Schmidt, J. Mathur, and A. E. Dubin. 2012. Piezo proteins are pore-forming subunits of mechanically activated channels. Nature 483:176-181.
49. Powers, R. J., S. Roy, E. Atilgan, W. E. Brownell, S. X. Sun, P. G. Gillespie, and A. A. Spector. 2012. Stereocilia membrane deformation: Implications for the gating spring and mechanotransduction channel. Biophysical journal 102:201-210.
50. Powers, R. J., S. Kulason, E. Atilgan, W. E. Brownell, S. X. Sun, P. G. Barr-Gillespie, and A. A. Spector. 2014. The Local Forces Acting on the Mechanotransduction Channel in Hair Cell Stereocilia. Biophysical journal 106:2519-2528.
51. Kawashima, Y., G. S. Géléoc, K. Kurima, V. Labay, A. Lelli, Y. Asai, T. Makishima, D. K. Wu, C. C. Della Santina, and J. R. Holt. 2011. Mechanotransduction in mouse inner ear hair cells requires transmembrane channel–like genes. The Journal of clinical investigation 121:4796.
#52. Beurg, M., J.-H. Nam, A. Crawford, and R. Fettiplace. 2008. The actions of calcium on hair

bundle mechanics in mammalian cochlear hair cells. Biophysical journal 94:2639-2653.

#53. Farris, H., C. LeBlanc, J. Goswami, and A. Ricci. 2004. Probing the pore of the auditory hair cell mechanotransducer channel in turtle. The Journal of physiology 558:769-792.

#54. Solmaz, M. E., S. Sankhagowit, R. Biswas, C. A. Mejia, M. L. Povinelli, and N. Malmstadt. 2013. Optical stretching as a tool to investigate the mechanical properties of lipid bilayers. RSC advances 3:16632-16638.

#55. de Monvel, J. B., W. Brownell, and M. Ulfendahl. 2006. Lateral diffusion anisotropy and membrane lipid/skeleton interaction in outer hair cells. Biophysical journal 91:364-381.

#56. Marguet, D., P.-F. Lenne, H. Rigneault, and H.-T. He. 2006. Dynamics in the plasma membrane: how to combine fluidity and order. The EMBO journal 25:3446-3457.

#57. Petrache, H. I., S. W. Dodd, and M. F. Brown. 2000. Area per Lipid and Acyl Length Distributions in Fluid Phosphatidylcholines Determined by< sup> 2</sup> H NMR Spectroscopy. Biophysical journal 79:3172-3192.

#58. Tirrell, M., and M. F. Malone. 1977. Stress-induced diffusion of macromolecules. Journal of Polymer Science: Polymer Physics Edition 15:1569-1583.

Unconventional mechanics of lipid membranes: a potential role for mechanotransduction of hair cells stereocilia

Jichul Kim,
Department of Mechanical Engineering, Stanford University, Stanford, California

Supporting Materials for:

"Unconventional mechanics of lipid membranes: a potential role for mechanotransduction of hair cells stereocilia" by Jichul Kim

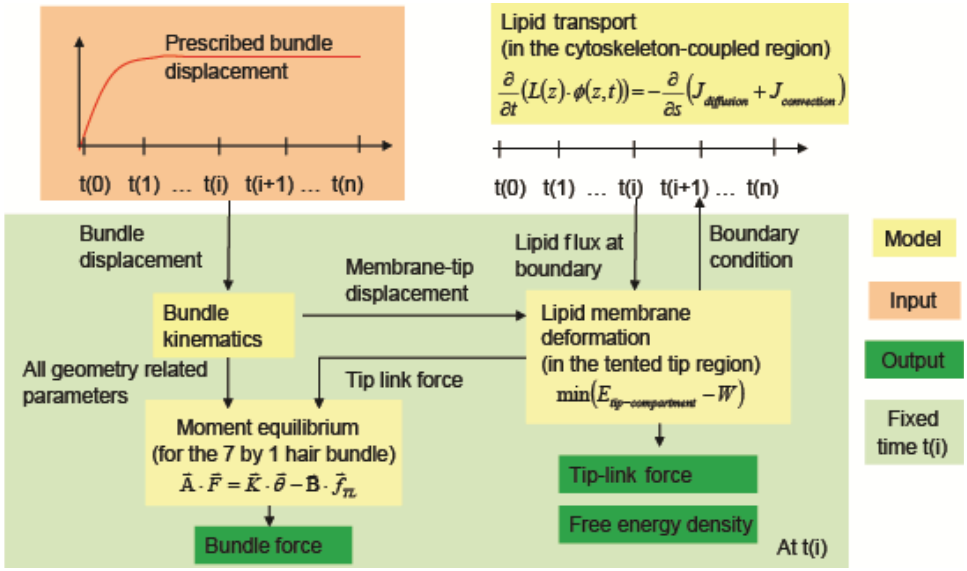

FIGURE S1 Multi-physics coupling. The presented multi-physics models are coupled and implemented using *Matlab* (www.mathworks.com). Briefly, for a given input bundle displacement, motion of the seven stereocilia that comprise a bundle row is determined by using the kinematics of the system based on the sliding shear motion of the bundle. Membrane-tip displacement, calculated from the bundle kinematics, is then taken as input for the lipid-membrane deformation over the tip region, which yields the tip-link force and membrane free energy density. Hydrodynamics lipid transport in the cytoskeleton-coupled region, which is a time-dependent initial and boundary-value problem, is solved in parallel with the lipid-deformation model and coupled through the interface boundary condition. The tip-link force becomes the input for the system equation to calculate the bundle force and forces applied to the side links. With this model, the temporal response of the tip-link force, hair-bundle force, and membrane free energy density at specific points in the tented tip compartment with respect to hair bundle motion can be computed. See Method section for descriptions of the equations

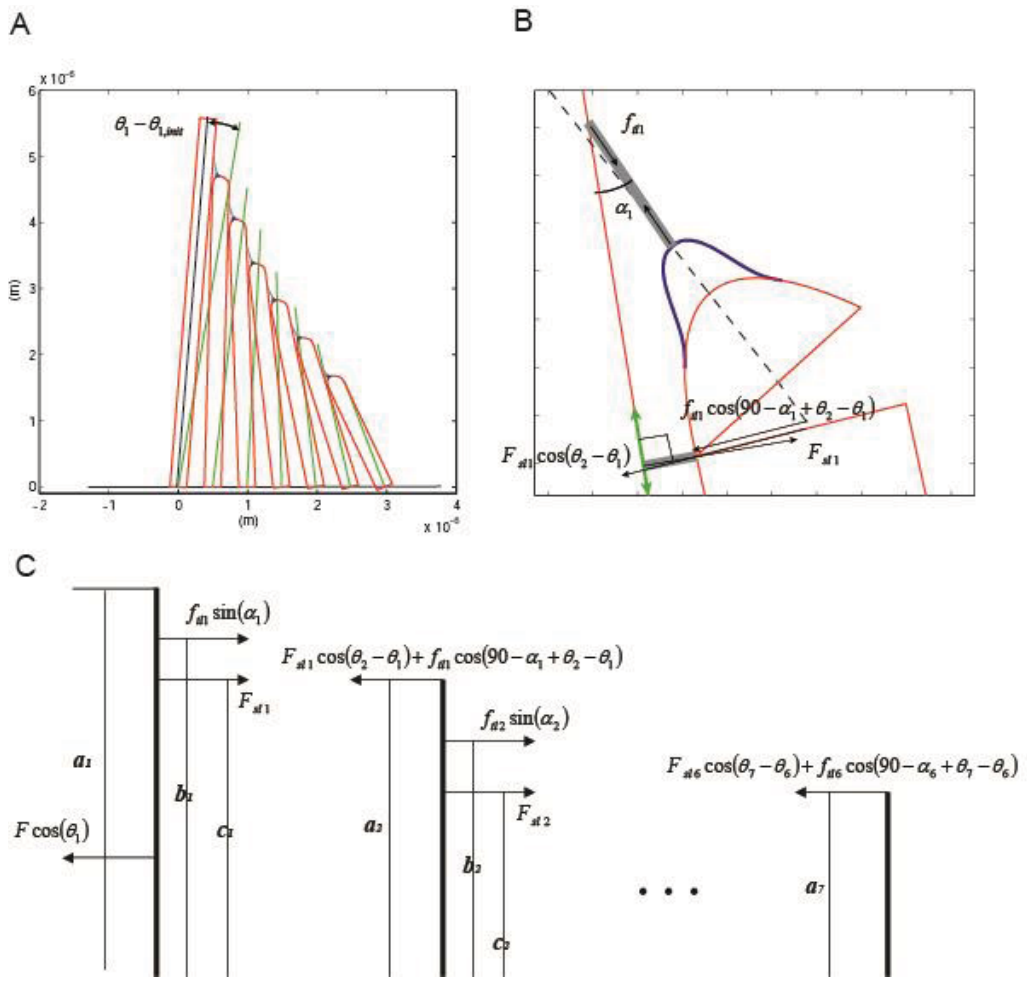

FIGURE S2 Kinematics component for the hair bundle model. (***A***) Hair bundle model configuration and dimensions. Green lines represent the initial resting central axis of each stereocilium. (***B***) Ciliary tip complex details and free body diagram. (***C***) Rotational free body diagram for the bundle's system equation. See Eq. 1 and Method section for a description of the parameters.

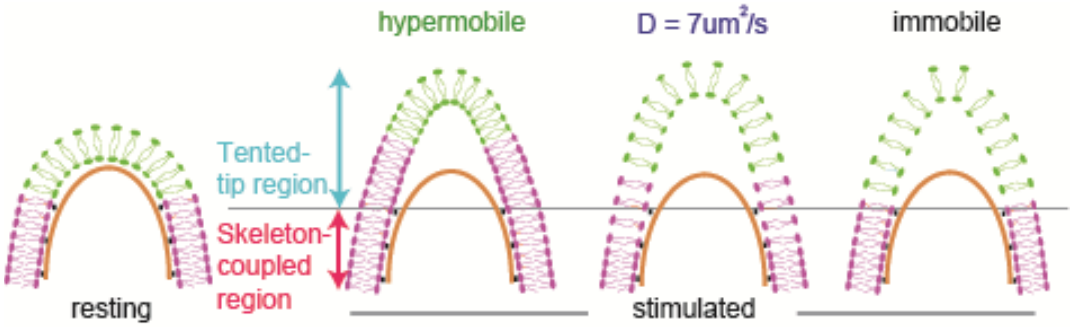

FIGURE S3 Illustration of the lipid flow in the stereocilia. Lipid flow in the cytoskeleton-coupled

region (red arrow) is more viscous than that of the tented tip region (blue arrow) due to the frictional interaction between mobile lipids and anchored crosslinkers (see Fig. S4b for a possible molecular configuration of the cytoskeleton-coupled region). When the membrane is pulled under point stimuli, lipid densities in two regions are constant temporally and spatially for the hypermobile case. However, in the case of physiologically relevant lipid mobility (with $D=7\ \mu m^2/s$), lower lipid density in the tented region and the density gradient in the cytoskeleton-coupled region are generated. Even though the case is physiologically and physically not relevant, the immobile case demonstrates the lowest lipid density in the tented region and an infinite gradient (i.e. discontinuity of the lipid density) at the interface. For all cases, the tented region is assumed to have a spatially uniform lipid density (i.e. quasi static). Two different colors for the lipid are used to trace the motion of the lipid with respect to the resting configuration. The thick brown line simply indicates the cytoskeleton i.e. actin core, and the thin black line indicates the interface between two regions of the lipid membrane.

Discussion for the parameters in the model

There are three types of parameters in this hair bundle model: parameters for the bundle, the ion channel, and the lipid membrane. First, the bundle parameters include the rotational stiffness of the rootlet and the geometric parameters demonstrated in Fig. S2. Since the rotational stiffness for the rootlet of the single stereocilium is unknown, this model parameter of 0.2 *fN/rad* is initially based on whole bundle measurements from rat outer hair cell bundles, where single stereocilia stiffness is calculated (1). This value is systematically adjusted to satisfy experimental force vs. displacement measurement from turtle with and without tip links. Second, the mechanosensitive ion channel parameters include area and internal energy difference between open and closed states of the channel. As mentioned in the main text, the internal energy difference of the hair cell MS channel is unknown, as the structural identity of the channel remains elusive. Therefore, we speculate on this free parameter of $7k_bT$ based on the energy of a typical MS ion channel (2). For estimating the area difference of the channel of 3 nm^2, the size difference of the channel pore between an open and close state measured from a turtle is used (3). Third, lipid bilayer material properties for the tiny tip part of the stereocilia has not been directly tested thus far, and therefore selection of those values for this predictive research is based on previous research for the vesicle

system or other cell types. The bending modulus for the lipid bilayer is in a range of 10-60k_bT (4-7) and it is closely correlated with the area stretching modulus, which is in a range of 110-650 *mN/m* (4, 5, 7). The nanoscopic diffusion constant for the tiny tip of the stereocilia also remains unknown. The confocal microscope measurement with 500 *nm* resolution estimates a microscopic diffusion constant of 1.1 $\mu m^2/s$ for the stereocilia (8). However, considering the tendency of underestimating the diffusion constant with low resolution experimental techniques (9), we expect that the nanoscopic diffusion constant for the stereocilia tip could be greater than the measurement in (8). Finally, the resting lipid areal density ϕ_0 is taken from (10).

Detailed formulation for Eq. 10: Convective flux of lipids in the cytoskeleton-coupled region

In the cytoskeleton-coupled region, the convective flux of the lipid with drift velocity υ to the tangential direction of the membrane can be first written as follows

$$J_{convection}(s,t) = L(s)\cdot\phi(s,t)\cdot\upsilon(s,t) \quad \text{[S1]}$$

where *s*, *L*, and ϕ are the coordinate of the curve, the circumferential length of the stereocilia, and the lipid area density respectively. As depicted previously in the main text and in Fig.S4b, the drift velocity of the lipid here is driven by inter-molecular potential interaction and may be able to be parameterized by using the surface tension of the membrane. To formulate convective flux of lipids in detail, three concepts can be taken in order. First, the center of mass at which force f_c for driving drift of lipids is applied must be specified. For this purpose, one simple but reasonable approach is to define the mass as a pair of lipids at upper and lower leaflets for which the center of mass is located in the neutral plane of the membrane (see Fig. S4b). The second step is to formulate the applied force f_c at the center of mass in terms of gradient of the surface tension. This formulation is faithfully depicted below but again non-uniform stretching of the membrane due to the membrane-skeleton interaction is the basis of this surface tension gradient. Finally, this applied force f_c satisfies the equilibrium condition with the viscous drag force in the form of $f_{drag} = -\upsilon/\mu = -f_c$. Here, the coefficient μ is the mobility of the lipid membrane (i.e. inverse of the drag coefficient) (11, 12).

To formulate $f_c(s,t)$ it is necessary to consider a sectioned membrane area with infinitesimal arc length δs, as shown in Fig. S4a. At a fixed time, the net tensile force applied at $s=s_1$ in the tangential direction of the arc length is $\sigma(s_1)\cdot L(s_1)$. Similarly, it is $\sigma(s_2)\cdot L(s_2)$ at $s=s_2$.

Since the number of lipids in the area from s_1 to s_2 i.e. $\int_{s1}^{s2} \phi(s) \cdot L(s) ds$ can be written as $\phi(s) \cdot L(s) \cdot \delta s$ when the infinitesimal arc length δs goes to zero, the tensile force applied for one center of mass at $s=s_1$ i.e. $f(s_1)$ can be calculated by normalizing the net force with respect to the number of center of mass in the sectioned area,

$$f(s_1) = \frac{2\sigma(s_1) \cdot L(s_1)}{\phi(s) \cdot L(s) \cdot \delta s} = \frac{2\sigma(s_1)}{\phi(s) \cdot \delta s} \quad \text{[S2]}$$

Here, in Eq. S2, "*2*" in the numerator represents two paired lipids at the upper and the lower leaflets for one center of mass. Similarly, the tensile force applied for one center of mass at $s=s_2$ is

$$f(s_2) = \frac{2\sigma(s_2)}{\phi(s) \cdot \delta s} \quad \text{[S3]}$$

From the general differential relationship for the quantity of σ along the arc length s as follows

$$\sigma(s_2) + \frac{\partial \sigma(s)}{\partial s} \cdot \delta s = \sigma(s_1) \quad \text{[S4]}$$

the applied force $f_c(s,t)$ can be expressed as follows in Eq. S5 by taking the difference of the tensile forces for the center of mass in the opposite direction (see Fig. S4 for the free body diagram).

$$f_c(s,t) = f(s_1,t) - f(s_2,t) = \frac{2\sigma(s_1)}{\phi(s) \cdot \delta s} - \frac{2\sigma(s_2)}{\phi(s) \cdot \delta s} = \frac{2}{\phi(s,t)} \frac{\partial \sigma(s,t)}{\partial s} \quad \text{[S5]}$$

The mobility of the lipid μ is parameterized with the diffusion constant by using the Einstein relation $\mu=D/(k_bT)$ (11-13). Finally, Eqs. S1 and S5 and the drift velocity of the form $\upsilon=-\mu f_{drag}=\mu f_c$ give the equation for the convective flux as follows

$$J_{convection}(z,t) = \frac{2D}{k_bT} L(z) \cdot \frac{\partial \sigma(z,t)}{\partial s} \quad \text{[S6]}$$

Here, k_b is Boltzmann's constant and T is temperature in Kelvin. The surface tension σ is a function of ϕ, which is given by Eq. 7.

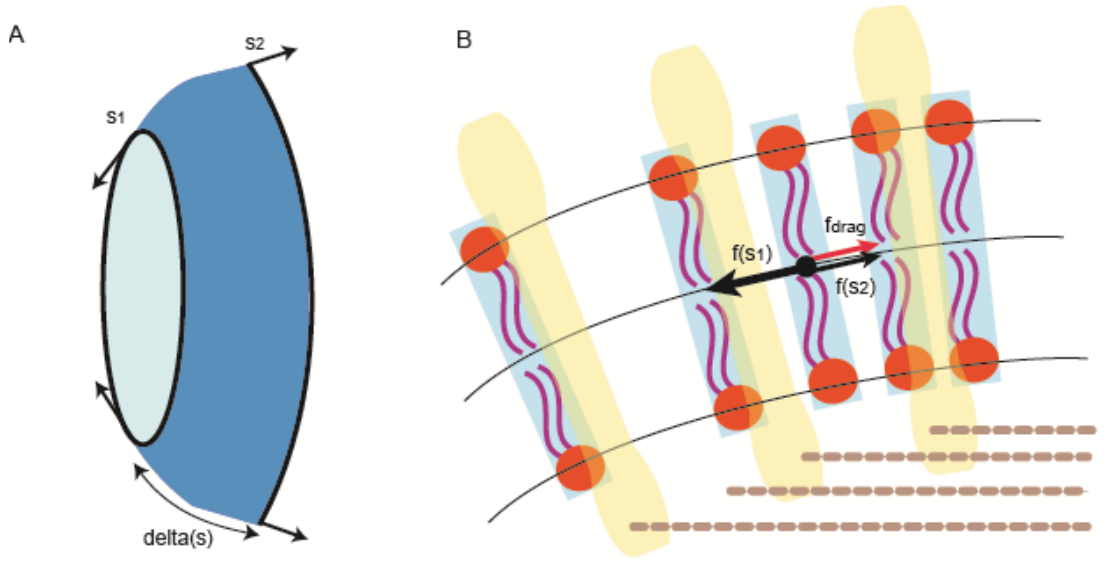

FIGURE S4 (***A***) Section of lipid membrane in the cytoskeleton-coupled region with infinitesimal arc length δs. Surface tensions at $s=s_1$ and $s=s_2$ are different when the membrane is non-uniformly stretched. (***B***) Paired lipids at the upper and the lower leaflets for which their center of mass (black dot) flows by following the neutral plane of the membrane. Thick-black and thin-black arrows indicate higher and lower tension applied on the center of mass in the opposite direction, respectively. The red arrow indicates viscous drag force in the opposite direction of the drift velocity. The viscous drag force is assumed to be generated by the interaction between lipids and crosslinkers (yellow) anchored to the cytoskeleton (dashed brown) (14). The difference between the two tensile forces (black arrows) lies in the force equilibrium with the drag force (red arrow), (i.e. $f(s_1)-f(s_2)=f_c=-f_{drag}$, where f_c is given by Eq. S5)

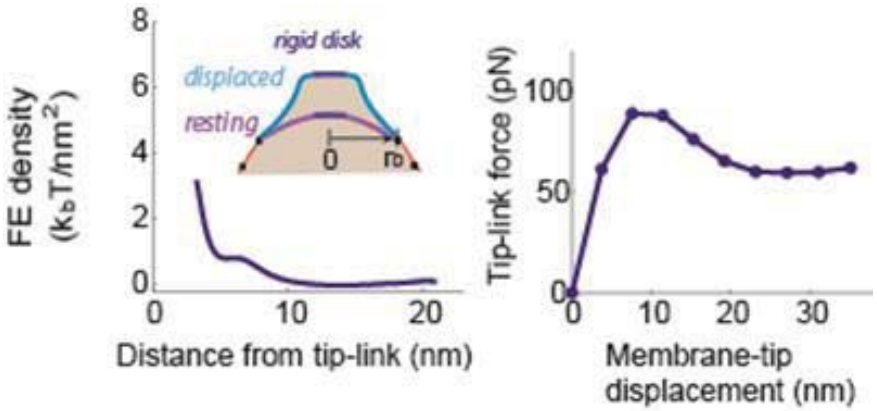

FIGURE S5 Potential effect of stiff membrane protein at center of the tip membrane. A rigid

disk of radius 3 *nm* is inserted. (Left) Tented-tip membrane free energy density profiles when the bundle is displaced by 38 *nm*. The high energy density region is shifted due to the rigid disk at the center. (Right) Tip link force vs. membrane-tip displacement response. Adding the rigid disk does not change the characteristic of the nonlinear response. The presented data are generated identically to the data in Fig. 2. All parameters are the same as those of Fig. 2 but r_b=24 *nm* is used here.

Supporting References

1. Beurg, M., J.-H. Nam, A. Crawford, and R. Fettiplace. 2008. The actions of calcium on hair bundle mechanics in mammalian cochlear hair cells. Biophysical journal 94:2639-2653.
2. Ursell, T., J. Kondev, D. Reeves, P. A. Wiggins, and R. RobPhillips. 2008. Role of lipid bilayer mechanics in mechanosensation. In Mechanosensitive Ion Channels. Springer. 37-70.
3. Farris, H., C. LeBlanc, J. Goswami, and A. Ricci. 2004. Probing the pore of the auditory hair cell mechanotransducer channel in turtle. The Journal of physiology 558:769-792.
4. Evans, E., and W. Rawicz. 1990. Entropy-driven tension and bending elasticity in condensed-fluid membranes. Physical Review Letters 64:2094.
5. Rawicz, W., K. Olbrich, T. McIntosh, D. Needham, and E. Evans. 2000. Effect of chain length and unsaturation on elasticity of lipid bilayers. Biophysical journal 79:328-339.
6. Powers, R. J., S. Roy, E. Atilgan, W. E. Brownell, S. X. Sun, P. G. Gillespie, and A. A. Spector. 2012. Stereocilia membrane deformation: Implications for the gating spring and mechanotransduction channel. Biophysical journal 102:201-210.
7. Solmaz, M. E., S. Sankhagowit, R. Biswas, C. A. Mejia, M. L. Povinelli, and N. Malmstadt. 2013. Optical stretching as a tool to investigate the mechanical properties of lipid bilayers. RSC advances 3:16632-16638.
8. de Monvel, J. B., W. Brownell, and M. Ulfendahl. 2006. Lateral diffusion anisotropy and membrane lipid/skeleton interaction in outer hair cells. Biophysical journal 91:364-381.
9. Marguet, D., P.-F. Lenne, H. Rigneault, and H.-T. He. 2006. Dynamics in the plasma membrane: how to combine fluidity and order. The EMBO journal 25:3446-3457.
10. Petrache, H. I., S. W. Dodd, and M. F. Brown. 2000. Area per Lipid and Acyl Length Distributions in Fluid Phosphatidylcholines Determined by< sup> 2</sup> H NMR Spectroscopy. Biophysical journal 79:3172-3192.
11. Hughes, B., B. Pailthorpe, and L. White. 1981. Translational and Rotational Drag on a Cylinder Moving in a Membrane. Journal of Fluid Mechanics 110:349-372.
12. Hochmuth, R. 1982. Solid and liquid behavior of red cell membrane. Annual review of biophysics and bioengineering 11:43-55.

13. Tirrell, M., and M. F. Malone. 1977. Stress-induced diffusion of macromolecules. Journal of Polymer Science: Polymer Physics Edition 15:1569-1583.
14. Kusumi, A., C. Nakada, K. Ritchie, K. Murase, K. Suzuki, H. Murakoshi, R. S. Kasai, J. Kondo, and T. Fujiwara. 2005. Paradigm shift of the plasma membrane concept from the two-dimensional continuum fluid to the partitioned fluid: high-speed single-molecule tracking of membrane molecules. Annu. Rev. Biophys. Biomol. Struct. 34:351-378.